Xenogenic Neural Stem Cell-Derived Extracellular Nanovesicles Modulate Human Mesenchymal Stem Cell Fate and Reconstruct Metabolomic Structure

Burak Derkus,[1,2*] Melis Isik,[2] Cemil Can Eylem,[3] İrem Ergin,[4] Can Berk Camci,[1] Sila Bilgin,[1] Caglar Elbuken,[5,6] Yavuz Emre Arslan,[7] Merve Akkulak,[8] Orhan Adali,[8] Fadime Kiran,[9] Babatunde O. Okesola,[10,11] Emirhan Nemutlu,[3,12] Emel Emregul[2]

[1] Stem Cell Research Lab, Department of Chemistry, Faculty of Science, Ankara University, 06560 Ankara, Turkey

[2] Interdisciplinary Research Unit for Advanced Materials (INTRAM), Department of Chemistry, Faculty of Science, Ankara University, 06560 Ankara, Turkey

[3] Analytical Chemistry Division, Faculty of Pharmacy, Hacettepe University, Ankara, Turkey

[4] Department of Surgery, Faculty of Veterinary Medicine, Ankara University, Turkey

[5] UNAM-National Nanotechnology Research Center, Institute of Materials Science and Nanotechnology, Bilkent University, Ankara, Turkey

[6] Faculty of Biochemistry and Molecular Medicine, Faculty of Medicine, University of Oulu, 90014 Oulu, Finland

[7] Regenerative Biomaterials Laboratory, Department of Bioengineering, Engineering Faculty, Çanakkale Onsekiz Mart University, Çanakkale 17100, Turkey

[8] Department of Biological Sciences, Faculty of Science, Middle East Technical University, Ankara, Turkey

[9] Department of Biology, Faculty of Science, Ankara University, 06560 Ankara, Turkey

[10] Institute of Bioengineering, Queen Mary University of London, London E1 4NS, U.K.

[11] School of Engineering and Materials Science, Queen Mary University of London, London E1 4NS, U.K.

[12] Bioanalytic and Omics Laboratory, Faculty of Pharmacy, Hacettepe University, Ankara, Turkey

Abstract

Extracellular nanovesicles, particularly exosomes, can deliver their rich bioactive biomolecular content including miRNAs, proteins and lipids, and thus providing a context for researching the capability of exosomes to induce stem cells toward lineage-specific cells and tissue regeneration. In this study, we demonstrate that rat subventricular zone neural stem cell-derived exosomes (rSVZ-NSCExo) can control neural-lineage specification of human mesenchymal stem cells (hMSCs). We use miRNA array analysis to show that the miRNA content of both rSVZ tissue and rSVZ-NSCExo are similar. Through immunocytochemistry, gene expression, and multi-omics analyses, we demonstrate the capability to use rSVZ-NSCExo to induce hMSCs into either a neuroglial or neural stem cell phenotype and genotype in a temporal and dose-dependent manner, and via multiple signaling pathways. The current study presents a new and innovative strategy to induce hMSCs into neural lineage by harnessing the rich molecular compositions of exosomes, thus suggesting future opportunities for rSVZ-NSCExo in nerve tissue regeneration.

Keywords: Exosomes, Extracellular Vesicles, Subventricular Zone, Neural Differentiation, Neural Stem Cells, Mesenchymal Stem Cells, Metabolomics

1. INTRODUCTION

Neurogenic differentiation is a dynamic process involving functional regulation of FoxO1[1], EZH2-mediated histone methylation by SOX19b[2], binding of neurotrophins to receptor tyrosine kinases (RTKs)[3], regulation of Rho-GDIγ by hepatic nuclear factor (HNF4-1), and myc-associated zinc finger protein (MAZ-1)[4]. Also, the induction of NGN2 expression by PAX6 is well-known to promote neuronal differentiation by repressing HES5 and inhibiting downstream Notch effectors[5]. Moreover, STAT3 and SMAD1 activation by interleukin-6 family that induces glial protein expression plays an important role in neurogenic differentiation [6]. In addition to transcriptional and epigenetic regulation, post-transcriptional mechanisms, largely mediated by miRNAs, also contribute to cell specification during neural differentiation [7, 8]. Several specific miRNAs are involved in different neurogenic processes such as neuronal migration[9], proliferation of neural stem cells (NSCs)[10, 11], and neural cell specification[12].

To induce neurogenic differentiation of mesenchymal stem cells (MSCs), inductive chemicals such as β-mercaptoethanol (bME) and retinoids have been demonstrated[13]. Growth factors, including epidermal growth factor (EGF), nerve growth factor (NGF)[14], and neurotrophins[15] have been prominently used to induce neurogenic gene expression. MSCs can also give rise to neural lineage cells and acquire neuronal phenotypes when induced with substances able to elevate intracellular level of cyclic adenosine monophosphate (cAMP). For example, forskolin and dibutyryl cAMP have been frequently used for neuronal differentiation of MSCs[16]. Despite the successful and continuous use of the aforementioned inductive factors, their uses are associated with certain drawbacks including (i) poor solubility in aqueous solutions, (ii) induction of autophagy and/or apoptosis[17], (iii) adverse cardiac remodeling[18], and (iv) adverse physiological action on the sensory and autonomic systems[19]. Consequently, an alternative approach to facilitate neurogenic differentiation of MSCs without displaying these limitations will represent a new direction and timely intervention in the field.

Emerging evidences have implicated the use of exosomes in cell differentiation[20, 21], cellular communication[22], disease diagnosis[23], and tissue regeneration[24] as an attractive and viable strategy in cell/tissue engineering. Despite being, a rich source of bioactive proteins (growth

factors), lipids, metabolites, and genetic materials (mRNAs, miRNAs, and noncoding RNAs) [25] that can stimulate cell differentiation, the use of exosomes for this purpose has rarely been explored[26-28]. Glioma-derived exosomes[26], exosomes isolated from neuronal cells[27], and differentiating neuronal cells[28] have been shown to induce MSCs and NSCs into neuron-like cells. However, the methods used for the isolation suffer some drawbacks including extremely low yield and that the neuron-like cells only showed neuritic extension. Exosome-mediated induction strategy has also been harnessed to induce MSCs into other tissue-specific cells including adipose and bone[29], nucleus pulposus[30], and odontogenic[31] cells. However, the underlying complex molecular mechanisms of exosome-triggered stem cell differentiation have not been fully elucidated.

In the current study, we use exosomes isolated from rat subventricular zone (rSVZ)- derived NSCs (rSVZ-NSCExo) to induce hMSCs into specific neural subtype cells due to their concentrated and innate biochemical contents and unique attributes such. NSCs-derived exosomes have been shown to regulate neurogenesis[32], attenuate apoptosis and neuroinflammation[33]. Moreover, Morton *et al.* previously demonstrated that NSCs in the SVZ regulate microglial morphogenesis in the central nervous system[34]. Considering this, we reasoned that NSCs-derived exosomes might induce MSCs differentiation into different neurogenic lineage cells. Herein, we report a growth factor/cytokine-free strategy for the xenogeneic exosome-mediated induction of hMSCs. This induction strategy enables a reliable neurogenic induction with a higher yield cell differentiation compared to previous reports by others, and enables the induction of MSCs differentiation into different subtypes of neural cells in a dose-dependent manner.

2. MATERIALS AND METHODS

2.1. Isolation and characterization of NSCs from rSVZ

We isolated NSCs from SVZ tissues[35] obtained from the brains of rats (n=9) as previously described[36] (Figure 1A,B). Briefly, Wistar Albino rats (6 months old, male) were euthanized using a protocol approved by the Institutional Animal Care and Use Committee of Canakkale On Sekiz Mart University (Turkey). The dissected brains were cut under a dissection microscope from ventral to dorsal between the left striatum and the left ventricle. Finally, SVZ-tissues were dislodged with a cut at the dorsal SVZ along the corpus callosum. The dislodged

SVZ tissues were kept in Hibernate A medium (Thermo Fisher, USA), a CO_2-independent medium for the maintenance of neural cells until further processed for NSCs isolation.

For NSC isolation, we dissociated SVZ tissues by pipetting, followed by treatment with trypsin–EDTA (0.05%) in Neurobasal A (Thermo Fisher, USA). After centrifugation, the obtained cell pellet was resuspended in N2B27 medium consisting of Neurobasal/DMEM-F12 (1:1) supplemented with GlutaMax (0.5% v/v), penicillin/streptomycin (1% v/v), epidermal growth factor (EGF, 10 ng/mL), fibroblast growth factor-2 (FGF-2, 20 ng/mL), N2 (1% v/v) and B27 (2% v/v). All media and supplements were obtained from Thermo Fisher, USA. The cells were then plated on laminin-coated 6-wells (200.000 cells/well).

We used various techniques for detailed characterization of the isolated cells. For the phenotypical analysis of rNSCs with flow cytometry, cells ($1x10^6$) were permeabilized with Triton X-100, blocked with bovine serum albumin (5%, BSA, Sigma-Aldrich, USA) in phosphate buffer saline (PBS), stained with Nestin antibody (1:200, Ab92391, Abcam, USA) and goat anti-rabbit IgG (1:1000, ab72465, Abcam, USA). We used flow cytometry (FACSAria, BD, USA) to analyze the stained cells.

Expression of Nestin and PAX6 in rNSCs, hMSCs (negative control), and rSVZ tissue (positive control) was investigated by quantitative reverse-transcriptase polymerase chain reaction (RT-qPCR, primers are listed in the SI). Total RNA was isolated from rNSCs, hMSCs, and rSVZ tissue using a commercial RNA isolation kit (GeneAll, Korea). To do this, we measured 100 ng of RNA on a Nanodrop (Nanodrop 2000/2000c, Thermo Fisher, UK) and reverse transcribed using a cDNA synthesis kit (Bio-Rad, USA) to obtain cDNA for each sample. For RT-qPCR, each reaction was run (Bio-rad CFX96 qPCR system, USA) in triplicate using SYBR green master mix, and the gene expressions were normalized to an internal control GAPDH.

The rNSCs were further characterized morphologically by immunofluorescent (IF) staining. The rNSCs were fixed with paraformaldehyde (PFA, 4% v/v), permeabilized with Triton X-100 (0.1% v/v), blocked with BSA (2% v/v), incubated with Nestin antibody (1:200), and finally labelled with goat anti-rabbit IgG secondary antibody with green fluorescence dye (Thermo Fisher, UK). The cell nuclei were stained with DAPI and cells were observed under a fluorescence microscope (Leica DMIL model, Leica, Germany).

We assessed the capability of rNSCs to form neurosphere by culturing the cells in ultra-low attachment 96-well plates (ULAP) for 3-4 days. In this case, cells ($2x10^4$) were seeded in N2B27 medium, and the formation of neurospheres was observed under an inverted phase/contrast microscope (Leica, Germany).

2.2. Isolation and characterisation of rSVZ-NSCExo

Conditioned media (CM) were collected from NSCs that we cultured up to 4 passages in laminin-coated 6-well plates in N2B27 medium. Exosomes from rSVZ-NSCs were isolated as described previously[23], but with a slight modification (Figure 2A). The collected CM was centrifuged for 15 min at 300 g and 4 °C to remove the cells. After filtration through 0.22 μm, CM was centrifuged at 2000 g and 12000 g at 4 °C to remove apoptotic bodies, microvesicles, and cell debris. Finally, CM was ultracentrifuge for 3h at 120000 g and 4 °C to pelletize the exosomes. The isolated exosomes were resuspended in PBS (10 mL) and re-pelletized to remove contaminants. The final product was dispersed in 100 μL of DPBS.

The rSVZ-NSCs derived exosomes were characterized with several techniques. Total protein was extracted from the rSVZ-NSCExo using a radioimmunoprecipitation assay (RIPA) buffer (Thermo Fisher, USA), and protein content was measured using a bicinchoninic acid (BCA) test (Thermo Fisher, USA) by recording the absorbance at 562 nm. For Western Blot (WB) analysis, the extracted proteins were separated by sodium dodecyl sulphate polyacrylamide gel (SDS-PAGE) electrophoresis, subsequently, transferred onto polyvinylidene difluoride (PVDF) membrane. The membrane was then blotted with exosome-specific antibodies namely CD9 and CD63 (1:200, Santa Cruz, USA), which was followed by incubation with horseradish peroxidase-conjugated anti-mouse IgG (1:2000, Abcam, UK). Proteins were then visualized using SuperSignal West Femto electrochemiluminescence (ECL) substrate (Bio-Rad, USA).

To analyze the morphological characteristics, rSVZ-NSCExo was counterstained and examined under transmission electron microscope (TEM). To this end, exosomes suspended in paraformaldehyde were pipetted (4 % v/v, 10 μL) onto the formvar-coated copper grids, allowed to settle by incubating for 10 min, further fixed with glutaraldehyde (1%, v/v) and stained with uranyl acetate (1%, w/v). After each step, the grid was washed with DPBS three times to remove remnants. Images were obtained using transmission electron microscopy (JEM100XC, JEOL Ltd., Japan). The size distribution of rSVZ-NSCExo was also assessed by dynamic light scattering (DLS), which measures the alterations of scattered light intensity

caused by the Brownian motion of the spherical particles. DLS spectra were obtained for rSVZ-NSCExo -that were diluted with DPBS (1:100 v/v)- using a Nanosizer (Malvern Instruments, Malvern, UK). Measurement was performed in triplicate.

Uptake of rSVZ-NSCExo by hMSCs is an important process for an effective cell differentiation. To investigate the cellular uptake of rSVZ-NSCExo, first we labelled the exosomes with PHK67 (Sigma Aldrich, USA) following the user manual, then incubate them with hMSCs culture (in 6-well plate), and finally observed under a fluorescence microscope (Leica DMIL model, Leica, Germany) using a 488 nm excitation wavelength.

2.3. miRNA array and metabolomics study to characterize molecular signatures of rSVZ-NSCExo

We used multi-omics analyses including miRNA array and metabolomics to obtain detailed miRNA and metabolite profiles of rSVZ-NSCExo.

To assess the similarity and differences in miRNA content of rSVZ tissue and rSVZ-NSCExo, miRNA microarray was conducted. rSVZ and exosomal miRNAs were extracted using miRNeasy Mini Kit (Qiagen, USA) in accordance with the manufacturer's instructions. The concentrations of miRNAs were measured with a spectrometer and the integrities were assessed using a Bioanalyzer (Agilent Technologies, USA). The miRNA profiles were obtained on an Affymetrix GeneChip miRNA 4.0 Array (Thermo Fisher, USA) having the capability to recognize 728 rat miRNAs. To examine the metabolite profiles of rSVZ-NSCExo, we extracted metabolites from SVZ-NSCExo and subjected to metabolomics analysis. Sample preparation and derivatization protocols are provided in the SI. The extracted metabolite samples were analyzed using a Gas Chromatography-Mass Spectrometry system (GC-MS-QP-2010 Ultra system, Shimadzu, Japan) with a DB5-MS column as well as liquid chromatography quadrupole time-of-flight mass spectrometry (LC-qTOF-MS). Data deconvolution and/or analysis for metabolomics study were conducted using several online tools as comprehensively described in SI.

2.4. Investigation of cytocompatibility of rSVZ-NSCExo

To assess the potential applicability of rSVZ-NSCExo as a cell induction agent, we conducted calcein-AM/ethidium homodimer-1 (EthD-1) staining to examine the cell viability before proceeding with further experiments. For this purpose, hMSCs were seeded in 96-well plates

($7.5x10^3$ cells/well) in a commercial expansion medium (Merck Millipore, USA) with exosome-depleted FBS (10%, v/v) (System Biosciences, USA) and penicillin/streptomycin (1%, v/v). Various concentrations (10, 50, and 100 μg/mL) of rSVZ-NSCExo were injected into the media 1 day after cell seeding. After definite culture periods (2 and 7 days), media were replaced with calcein-AM/EthD-1 solution (4 μM, Molecular Probes, Thermo Fisher, UK), and cell viability was observed under a fluorescence microscope (Leica DMIL model, Leica, Germany) using green (ex. 488 nm) and red (ex. 527 nm) channels. In addition, 3-(4,5-dimethylthiazol-2-yl)-5-(3-carboxymethoxyphenyl)-2-(4-sulfophenyl)-2H-tetrazolium (MTS) testing was conducted to investigate the effect of rSVZ-NSCExo on cell proliferation. These experiments were conducted with the same exosome concentrations and in the same conditions with the cell viability assay. After definite time points (2 and 7 days), the waste medium was discarded, and 20 μL of MTS reagent was added in each well containing 100 μL of fresh culture medium. After 1 h incubation in the dark at 37 ^oC, absorbance values were recorded at 490 nm. Each parameter was studied in triplicate. Tukey's multiple comparison test was used for the statistical evolution and comparison of groups.

2.5. rSVZ-NSCExo mediated reprogramming of hMSCs

The neuro-inductive potential of rSVZ-NSCExo on hMSCs was assessed by seeding cells in 6-well plates ($5x10^4$ cell/well) in the presence DMEM medium supplemented with FBS (10%, v/v) and P/S (1%, v/v) (denoted as growth medium, GM), and cultured for 1 day in order to ensure cell adhesion and spreading. On the following day, the media were discarded and replaced with DMEM medium with exosome-depleted FBS (2%, v/v) which was supplemented with rSVZ-NSCExo in different concentrations (10, 50, 100 μg/mL). Here, hMSCs that were cultured in GM and N2B27 medium were used as negative and positive controls, respectively.

The potential of rSVZ-NSCExo to induce hMSCs into neural-lineage cells was investigated phenotypically with IF staining. hMSCs, that were induced with rSVZ-NSCExo (10, 50, and 100 μg/mL) for 10 days, were immunostained with antibodies Nestin (1:200, Abcam, USA), SOX2 (1:200, Abcam, USA), GFAP (1:200, Thermo Fisher, USA), and Vimentin (1:200, Santa Cruz Biotechnology, USA) following the method described in the Section 2.1. Following secondary staining with goat anti-mouse IgG or goat anti-rabbit IgG, cells were observed under a fluorescence microscope (Leica DMIL model, Leica, Germany). To further assess the neuro-inductive potential of rSVZ-NSCExo, expressions of Nestin, GFAP, SOX2, PAX6, and Nestin

in rSVZ-NSCExo induced hMSCs were investigated by RT-qPCR following the protocol described in the Section 2.1 (primers have been listed in SI). In this case, hMSCs cultured in GM were used as the negative control, while hMSCs cultured in N2B27 were considered as the positive control. The differences between expression levels among groups were evaluated with a one-way ANOVA test; p-values< 0.05 were considered significant.

2.6. Optimization of the exosome-mediated neurogenic differentiation approach

To optimize the rSVZ-NSCExo based cell induction protocol, the effects of initial cell density and exosome loading frequency were investigated. For this purpose, rSVZ-NSCExo (100 μg/mL) was injected into the 6-wells in which hMSCs were cultured in different cell densities ($5x10^4$, $1x10^5$, and $2x10^5$ cells per 6-well). Culture media were refreshed every 3 days. To assess the effect of the exosome loading frequency, rSVZ-NSCExo (100 μg/mL) was loaded to the cell culture ($5x10^4$ cell per 6-well) 1, 2, and 3 times with 3-days' intervals. At the end of the 10-day induction period, neurogenic gene expressions were investigated with RT-qPCR for Nestin, SOX2, PAX6, GFAP, MAP2, and Vimentin. The differences between expression levels among groups were evaluated with a one-way ANOVA test; p-values< 0.05 were considered significant.

2.7. Assessment of rSVZ-NSCExo-mediated reprogramming strategy using multi-omics approach: miRNA profiling and metabolomics

Mechanism of action of the rSVZ-NSCExo mediated reprogramming of hMSCs into neural-lineage cells was deeply investigated with a multi-omics approach, including miRNA array and metabolomics. In this case, miRNA profile of hMSCs was compared with the miRNA profile of rSVZ-NSCExo (100 μg/mL)-induced hMSCs. In addition, metabolomics patterns of hMSCs induced with different concentrations of rSVZ-NSCExo (10, 50, and 100 μg/mL) were obtained. For a time-resolved mechanical understanding, we also performed metabolomics analyses for 1, 3, 5, and 10-days of exosomal induction. miRNA array and metabolomics analyses were performed as described in the Section 2.3. Additional notes on bioinformatics analyses were provided in SI.

3. RESULTS

3.1. Rational of the study

It is well-known that the therapeutic benefits of stem cells are largely driven by their paracrine factors. Increasing evidence showed that exosomes derived from stem cells might be the major source of these paracrine factors. Therefore, understanding the inductive capability of exosomes in various subtype of stem cells is far-reaching. Our strategy aims to characterize the molecular components and biological potential of rSVZ-NSCs derived exosomes and to harness the innate biochemical cues to induce mesenchymal stem cells differentiation into neural lineage cells with a reliable method. Exosomes were collected from xenogenic NSCs which we isolated from rSVZ (Figure 1A,B). After a comprehensive characterization process including miRNA profiling, rSVZ-NSCExo was used for the induction of hMSCs. Herein, we hypothesized that rSVZ-NSCExo can trigger neurogenic mRNA expression in hMSCs employing their genetic materials including miRNAs. Also, they can switch fibroblastic morphology to the unique morphologies of neural cells by employing the protein content of rSVZ-NSCExo that regulates neurogenesis. As such, we believe that rSVZ-NSCExo holds great potentials as a better substitute for pure growth factors and cytokines in regenerative medicine.

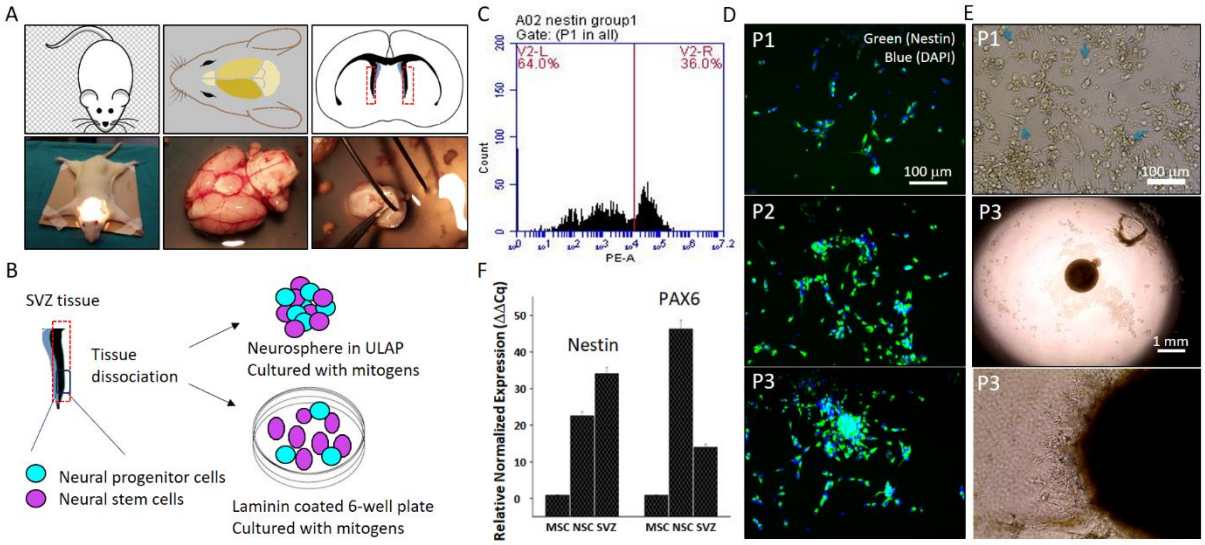

Figure 1. **Isolation of rSVZ-derived NSCs.** (A) Schematic representation and corresponding real images of the dissected rSVZ tissue. (B) Illustration of NSC isolation from rSVZ tissue. (C) Flow-cytometry diagram for Nestin+ NSCs. (D) rSVZ-NSCs at passage 1, 2, and 3, stained with Nestin and DAPI. (E) rSVZ-NSCs as monolayer culture (P1) and spheroid culture (P3). The cells when cultured onto Laminin-coated plate were shown to spread and form neuronal extensions. (F) Gene expression study for Nestin and PAX6, two neural stem cell markers, in comparison to hMSCs (negative control) and rSVZ (positive control). All experiments were performed thrice.

3.2. Isolation and characterization of NSCs

To identify rSVZ derived NSCs, we carried out flow cytometry analysis for Nestin. It was quantitatively shown that 36% of the SVZ-derived and isolated cells were Nestin-positive (Figure 1C). This isolation yield was found somewhat higher than those previously reported by others[37,38]. Immunofluorescence staining for Nestin further confirmed that the isolated cells have the characteristic phenotype of NSC (Figure 1D). The density of Nestin+ cells at the first passage was very low due to the presence of other neural-lineage cells, however, the density of Nestin+ cells increases with increasing passage number. In the third passage, almost all the cells exhibited Nestin+ phenotype (Figure 1D). This is possibly resulted from the elimination of non-neural stem cells because of their low proliferating capability. In addition to the flow cytometry and immunocytochemistry results, the ability of the isolated cells to form neurosphere was assessed. We observed the production of neurospheres (diameter ~1 mm) when the isolated cells were cultured in N2B27 medium supplemented with bFGF and EGF, which further confirmed the identity of the isolated cells (Figure 1E). When the obtained neurospheres were cultured with hMSCs on Laminin/Poly-L-Ornithine-coated wells in N2B27 in the absence of bFGF and EGF, formation of extended neurite-like branches (Figure 1D) that is characteristic of neuronal differentiation was observed. We then carried out gene expression analysis to probe the expression of two NSC-specific genes, Nestin and PAX6. NSCs exhibited a high-level expression for both Nestin and PAX6 when compared to the negative control hMSCs (Figure 1F). Unsurprisingly, the expression level of Nestin in SVZ tissue was higher than NSCs.

3.3. Characterization of rSVZ-NSCExo

The total protein content of rSVZ-NSCExo was calculated to be 5 mg/mL. The TEM micrograph of rSVZ-NSCExo showed many cup-shaped and stained wall nanovesicles with diameters between 50 and 200 nm, which is a typical size distribution for exosomes (Figure 2B). The TEM micrograph was consistent with the DLS data, which confirmed that rSVZ-NSCExo have a mean diameter of 80 nm (Figure 2C). The presence of two ubiquitous exosomal surface proteins (CD9 and CD63)[29, 39], which were detected by immunoblotting, further proved the identity of rSVZ-NSCExo (Figure 2D).

The uptake of exosomes by the cells is an important parameter for an efficient induction and cell reprogramming. Hence, we assessed the uptake of rSVZ-NSCExo by hMSCs by co-culturing PKH67-labeled exosomes with hMSCs. The green fluorescence signal of PKH67-labeled exosomes was apparent 30 min after the injection of exosomes (Figure 2E). At this time

point, individual exosomes or exosomal aggregates were recognizable. Also, an intense signal resulting from excessive uptake after 60 min was observed. These findings are consistent with the previous studies that reported the kinetics of exosomes' cellular uptake[40, 41]. This cellular uptake is vital for an efficient paracrine effect of the exosomes.

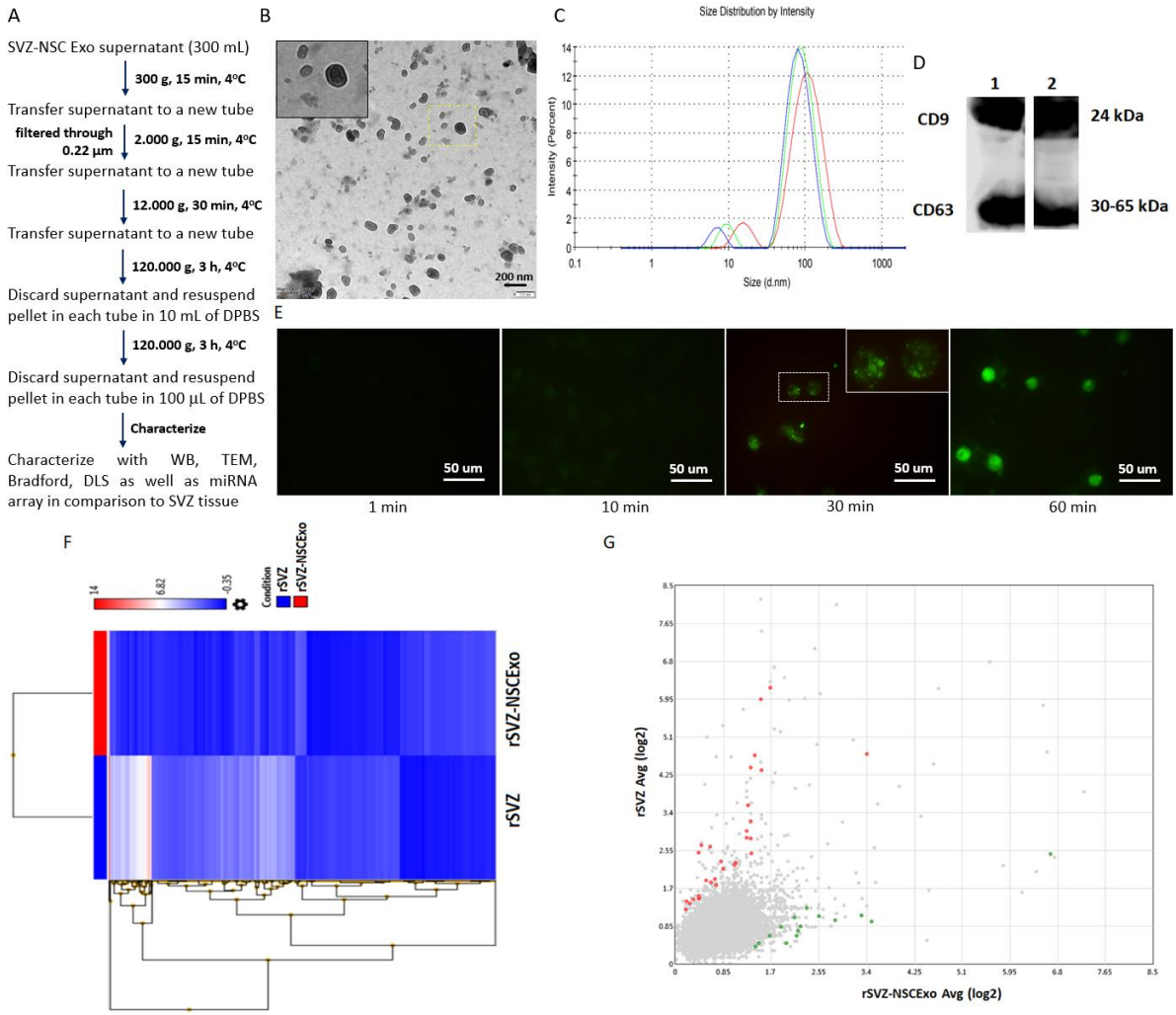

Figure 2. Isolation of rSVZ-NSCExo. (A) The protocol applied to rSVZ-NSC spent media to isolate exosomes. (B) TEM image showing the cup-shape exosomes with 50-200 nm diameter. (C) DLS spectrum exhibiting the size distribution for rSVZ-NSCExo (n=3). (D) Immunoblotting bands for CD9 and CD63, two exosomal surface proteins (n=2). (E) Tracking the time-dependent uptake of PKH67-stained rSVZ-NSCExo by hMSCs. (F) Hierarchical clustering of miRNA profile of rSVZ-NSCExo in comparison to rSVZ tissue (n=3). (G) Scattering graph obtained with significantly differentially expressed miRNAs in rSVZ-NSCExo as compared to rSVZ tissue (n=3). Red and green dots represent highly expressed miRNAs in rSVZ and rSVZ-NSCExo, respectively.

3.4. Exploring the molecular content of rSVZ-NSCExo

Elucidation of the biomolecular content of exosomes derived from primary cells represents a useful strategy to identify key biomolecular component that drives specific cellular processes under physiological conditions. To this end, we sought to determine the similarity between miRNA profiles of rSVZ tissue and rSVZ-NSCExo.

Hierarchical clustering (Figure 2F) and scattering (Figure 2G) analysis showed a significant overlap in the miRNA expressions of both rSVZ tissue and rSVZ-NSCExo (684 miRNAs). Some rat origin miRNAs (28 out of 728 miRNAs) in both cases were determined to be significantly up/down-regulated (change ≥2- fold, $p \leq 0.05$, listed in Table S1). This finding suggests that the isolated exosomes reflect the innate miRNA content of rSVZ tissue and can be used in cell reprogramming. This result shows for the first time that miRNA contents of exosomes and the corresponding tissues are identical. We then performed gene ontology analysis for the significantly up/down-regulated miRNAs in conjunction with FunRich3.0 (Entrez IDs are presented in Table S2) to show that the exosomes are enriched with nerve tissue-related miRNAs (Figure S1A). Furthermore, the enriched miRNAs regulate different biological processes including cell communication, signal transduction, and regulation of nucleic acid metabolism (Figure S1B) with receptor binding activity, GTPase activity, protein serine/threonine kinase activity, and transcription factor activity (Figure S1C). This result is consistent with previous reports[42, 43].

To identify rSVZ-NSCExo-enriched metabolites prior to downstream applications, we performed a combined GS-MS and LC-MS analyses. Amongst the whole metabolome, we identified 122 metabolites over the threshold (the list is available in Excel I file). Amongst the numerous metabolites, dopamine[44], betain[45], sphinganine[46], cholesterol[47], docosapentaenoic acid[48], and hypotaurine[49] are known to take part in neurogenesis or neural system functions. This finding supports the miRNome data and implies that rSVZ-NSCExo carries innate neurogenic materials. The obtained metabolome data also strengthen our hypothesis questioning the neuro-inductive potential of rSVZ-NSC-derived exosomes.

3.5. Cell biocompatibility of rSVZ-NSCExo

To assess the potential cytocompatibility of rSVZ-NSCExo, we conducted calcein-AM and ethd-1 staining as well as MTS testing for different doses of rSVZ-NSCExo (10, 50, and 100 μg/mL) to examine the cell viability and proliferation. Both microscopy (Figure S2A) and MTS

assay (Figure S2B) confirmed that rSVZ-NSCExo did not elicit obvious cytotoxic effect when applied between 10-100 μg/mL. This concentration range is consistent with concentrations we tested for neurogenic induction of hMSCs.

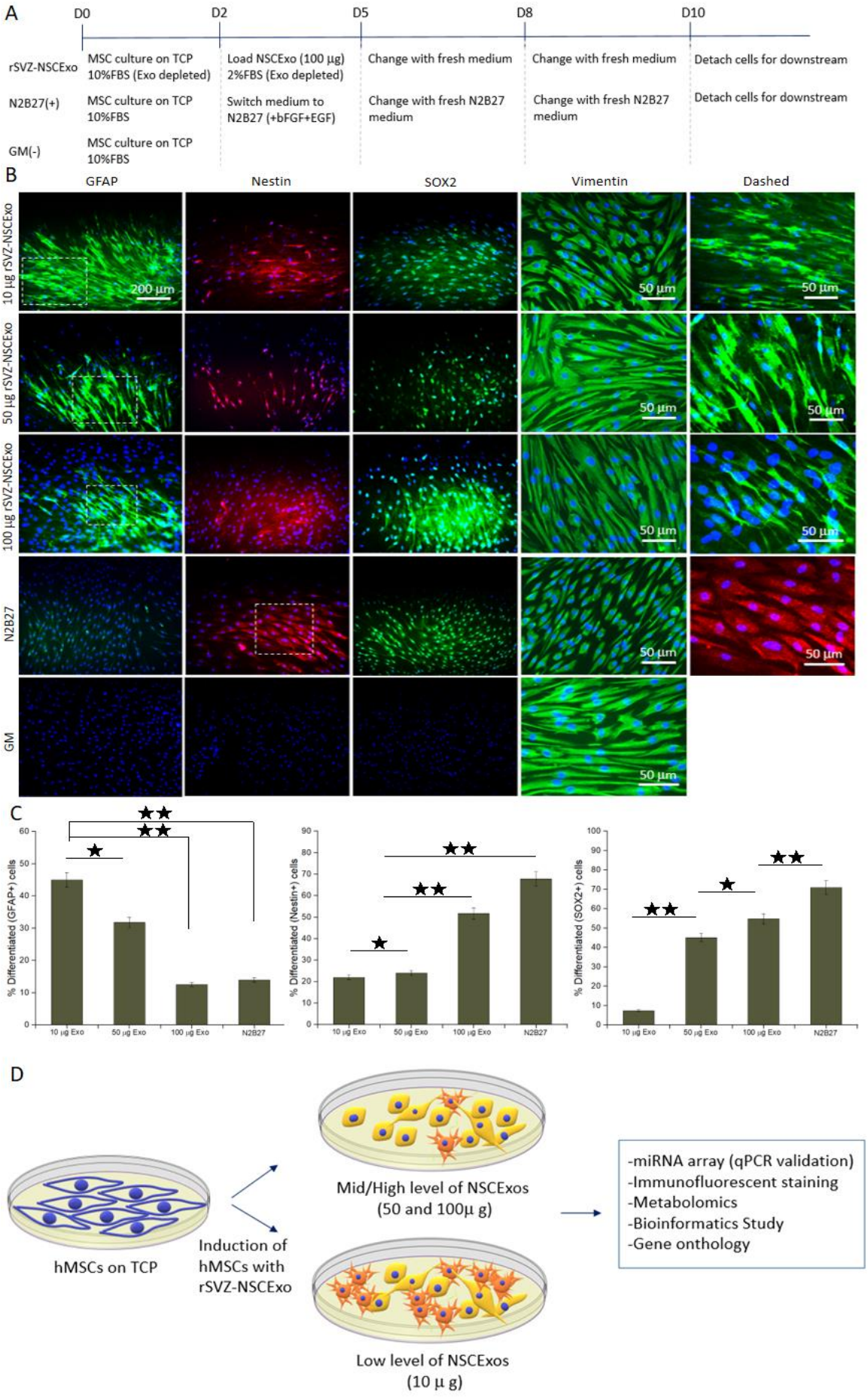
A
D0
D2
D5
D8
D10
rSVZ-NSCExo
MSC culture on TCP 10%FBS (Exo depleted)
Load NSCExo (100 µg) 2%FBS (Exo depleted)
Change with fresh medium
Change with fresh medium
Detach cells for downstream
N2B27(+)
MSC culture on TCP 10%FBS
Switch medium to N2B27 (+bFGF+EGF)
Change with fresh N2B27 medium
Change with fresh N2B27 medium
Detach cells for downstream
GM(-)
MSC culture on TCP 10%FBS
B
GFAP
Nestin
SOX2
Vimentin
Dashed
10 µg rSVZ-NSCExo
50 µg rSVZ-NSCExo
100 µg rSVZ-NSCExo
N2B27
GM
200 µm
50 µm
C
% Differentiated (GFAP+) cells
% Differentiated (Nestin+) cells
% Differentiated (SOX2+) cells
10 µg Exo
50 µg Exo
100 µg Exo
N2B27
D
hMSCs on TCP
Induction of hMSCs with rSVZ-NSCExo
Mid/High level of NSCExos (50 and 100µ g)
Low level of NSCExos (10 µ g)
-miRNA array (qPCR validation)
-Immunofluorescent staining
-Metabolomics
-Bioinformatics Study
-Gene onthology

Figure 3. Characterization of cell reprogramming through immunostaining. (A) Schematic of the culture system. (B) Immunofluorescence staining of rSVZ-NSCs-induced (10, 50, and 100 μg/mL) hMSCs for glial (GFAP) and NSC markers (Nestin and SOX2). Vimentin staining was performed for the assessment of cell phenotypes. The cells induced with N2B27 medium were considered as positive control while non-treated hMSCs were used as negative control. (C) The graphes indicate GFAP+, Nestin+, and SOX2+ cell ratios. (D) The illustration summarizes the proposed strategy and shows the downstream applications.

3.6. rSVZ-NSCExo reprograms hMSCs into neuroglial or neural stem cell pheonotype and genotype in a dose-dependent manner

Tissue-specific EVs are enriched in RNAs and proteins able to influence cellular processes, just like transcription factors do, and thereby regulate stem cell fate[29, 50]. Considering this, we hypothesized that exosomes obtained from rSVZ-NSCs contain numerous biomolecules that can induce cell differentiation or direct cell fate-decision. To test this hypothesis, we incorporated rSVZ-NSCExo (10, 50, and 100 μg/mL) into hMSCs medium and maintained the culture up to 10 days (Figure 3A). Immunofluorescence microscopy was used to probe two NSC markers (Nestin and SOX2), a neuroglial marker (GFAP), and a marker that is associated with the skeleton (Vim). Morphological observations showed that a high level (100 μg/mL) of rSVZ-NSCExo switched the fibroblastic morphology of hMSCs into a less spread/more rounded morphology of NSCs (Figure 3B). The cells were highly Nestin+ (52%) and SOX2+ (58%) positive but exhibited lower level of GFAP+ (12%) morphology (Figure 3C). When the rSVZ-NSCExo concentration was reduced to 50 μg/mL, the percentage of Nestin+ and SOX2+ cells decreased to 24% and 46%, respectively. In contrast, the percentage of GFAP+ cells increased to 31%. Interestingly and unexpectedly, in the presence of a very low concentration of rSVZ-NSCExo (10 μg/mL), a massive increase in GFAP+ cells (45%) was observed, whereas the percentage of Nestin+ and SOX2+ cell was restrained with 21% and %7, respectively. Similar to the observed neuro-inductive property of rSVZ-NSCExo, hMSCs cultured in N2B27 are highly differentiated into NSCs with high Nestin+ (70%), SOX2+ (69%) cell ratio and very low GFAP+ cell ratio (~ 10%) as expected. On the other hand, hMSCs cultured in GM retained their fibroblastic phenotype. Taking together, our results shows that rSVZ-NSCExo can regulates hMSCs' fate in a dose-dependent manner (Figure 3D). In light of previous studies[51], we speculate that this lineage-specification results from the rich exosomal content of rSVZ-NSCExo. NSC-specification derives from rSVZ-NSCExo's ability to transform cells where the exosomal content is sufficient at higher doses. On the other hand, at a lower dose the cells undergo random differentiation after a certain point. This observation suggests that hMSCs are reprogrammed by rSVZ-NSCExo in a dose-dependent manner.

Similar results demonstrating that exosomes modulate and differentiate stem cells in a dose-dependent manner have been previously reported for stimulation of neural progenitor cells[52] and Schwann cells[53].

To corroborate the immunocytochemistry results, we investigated mRNA expression of neural markers (Nestin, SOX2, GFAP) in hMSCs following the induction with rSVZ-NSCExo. When we treated hMSCs with high dose of rSVZ-NSCExo (100 μg/mL), we observed a significant expression of Nestin (by 6.7-fold, $p<0.05$) and SOX2 (by 3.1-fold, $p<0.05$) relative to the non-treated hMSCs (Figure 4A). Remarkably, expression levels of Nestin and SOX2 following the treatment with rSVZ-NSCExo (100 μg/mL) were similar to those obtained by culturing the cells in the N2B27 medium (positive control). A decrease in the level of Nestin expressions was observed with decreasing concentration of rSVZ-NSCExo (50 μg/mL) by 1.1-fold, but the decrease was not significant ($p>0.05$). However, SOX2 expression was decreased in rSVZ-NSCExo (50 μg/mL) treatment condition by 1.67-fold, indicating a significant change in SOX2 expression ($p<0.05$). On the other hand, GFAP expression was noticeably upregulated only in the cells treated with a low dose of rSVZ-NSCExo (10 μg/mL). In contrast, hMSCs that were cultured in N2B27 did not exhibit GFAP expression. Surprisingly, the expressions of Nestin and SOX2 were found to be insignificantly lower in D10 when compared to D3, which might have resulted from Nestin+SOX2+ cell death or random differentiation of hMSCs-derived NSCs (Figure 4B). The GFAP expression was significantly higher by 1.43-fold ($p<0.05$) at day 10 compared to day 3.

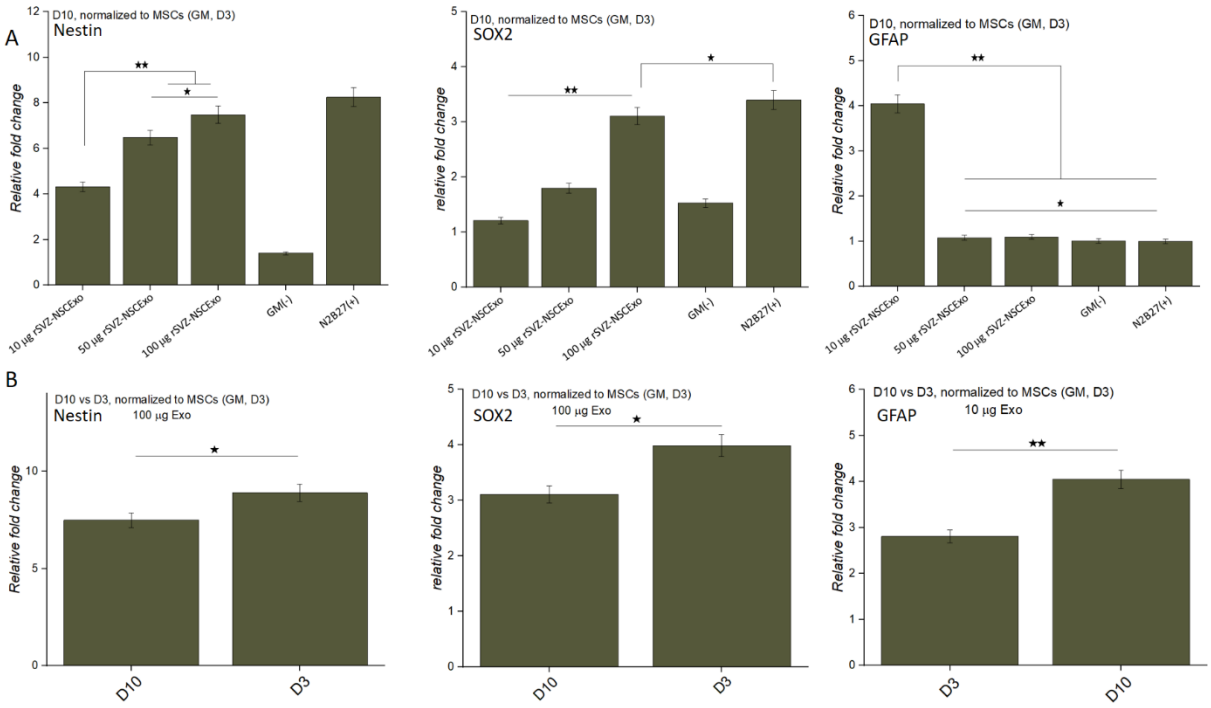

Figure 4. Characterization of neurogenic induction of hMSCs via rSVZ-NSCExo (n=3, technical replicate=3). (A) RT-qPCR graphes related to the expressions of Nestin, SOX2, and GFAP (A). Alterations of Nestin, SOX2, and GFAP expressions with time (B). N2B27-induced hMSCs and non-treated hMSCs were used as positive and negative controls, respectively. *p>0.05, **p<0.05.

To optimize the rSVZ-NSCExo assisted reprogramming of hMSCs into neural-lineage cells, we deeply investigated the optimal cell density and exosome loading protocol. To this end, rSVZ-NSCExo assisted reprogramming protocol was applied to different initial cell densities ($5x10^4$, $1x10^5$, and $2x10^5$ cells per 6-well). In this case, we found that lowest initial cell density ($5x10^4$) provided the highest Nestin expression, and the level of expression was gradually decreased when cell density was increased (Figure 5A). On the other hand, the expression of SOX2 and PAX6 was insignificantly changed when cell density was increased to $1x10^5$, whereas their expressions were seen to decrease when the cell density was further increased. Given the high rSVZ-NSCExo concentration (100 µg/mL) applied in these experiments, as expected, the expression of GFAP was not significant in all conditions. A similar result that showed the down-regulation of NSC-specific genes with increasing initial cell density has been reported by others[54]. This might also be attributed to the likelihood of a decreasing percentage of differentiated cells with increasing number of cells beyond an optimum density. To decipher the involvement of neuronal differentiation, which might be one of the reasons for the decreased expression level of NSC-specific genes, we investigated the expression of MAP2 in the same conditions. The expression of MAP2 was found insignificant (Figure 5A). To further explore

the underlying factors for the perturbed neural gene expressions, we performed a gene expression analysis for vimentin, which is a class-III intermediate filament found in non-epithelial cells, especially mesenchymal cells. The expression of vimentin appeared to be higher when the initial cell density was increased to some extent (from $5x10^4$ to $1x10^5$), indicating a higher mesenchymal character at the initial cell density of $1x10^5$. Whereas, it decreased when the cell density was further increased ($2x10^5$). This decrease in vimentin expression in higher cell density might be due to contact inhibition.

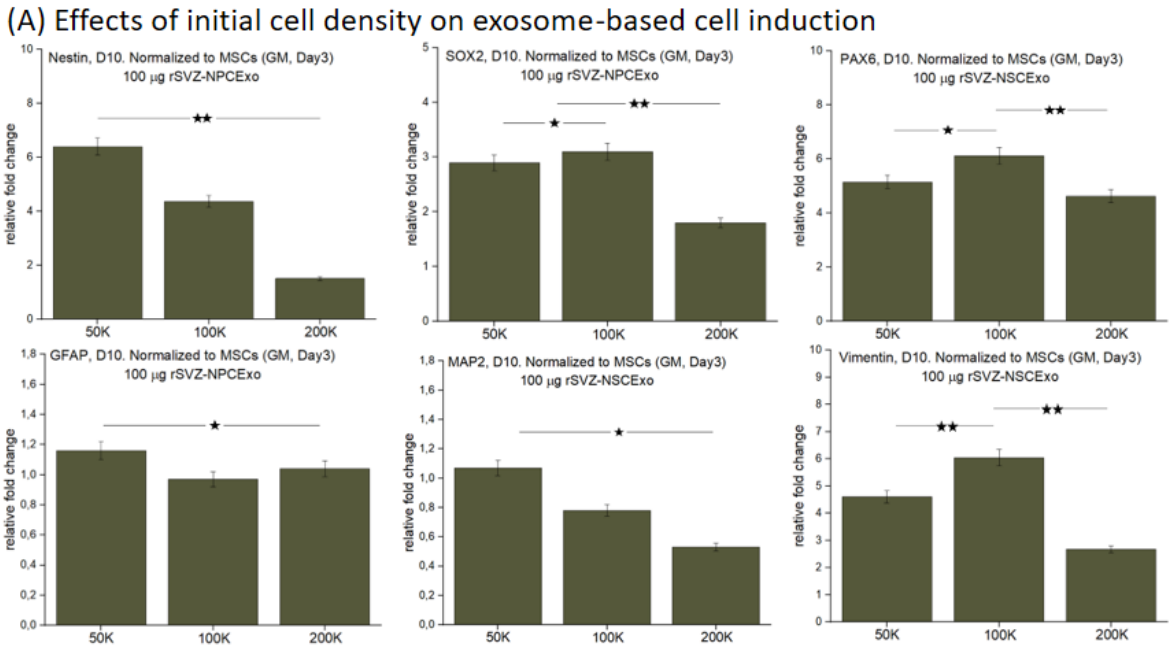

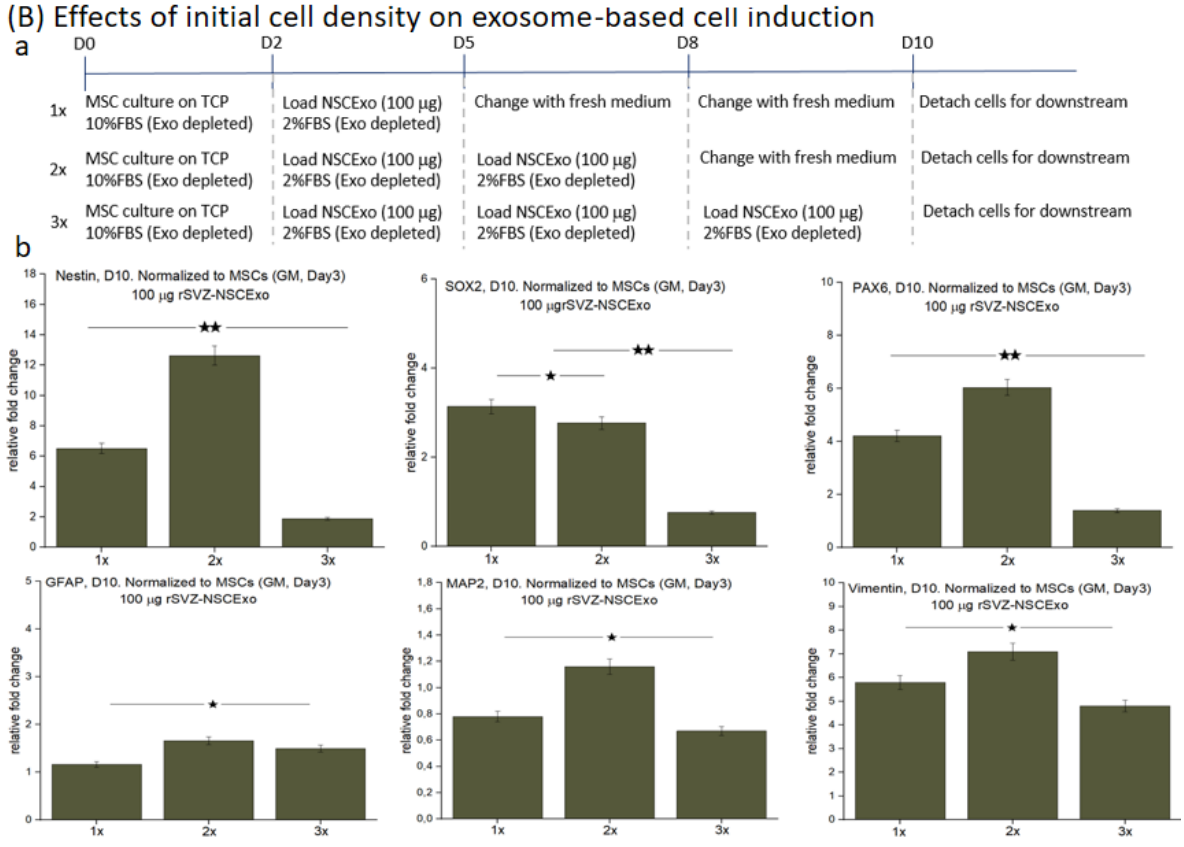

Figure 5. Optimization of cell reprogramming. (A) Effect of cell density (50K, 100K, and 200K) on rSVZ-NSCExo mediated neurogenic differentiation of hMSCs. (B) (a) Schematic presentation of reprogramming condtions. (b) Effect of exosome loading frequency (1, 2, and 3 times with 3 days' intervals) on rSVZ-NSCExo mediated neurogenic differentiation of hMSCs. All experiments were performed thrice with technical replicates (n=3). *p>0.05, **p<0.05.

To further validate the rSVZ-NSCExo assisted reprogramming protocol, we evaluated the expressions of genes following the treatment of hMSCs with three different time interval and loading regimes (Figure 5Ba). The results showed that expressions of all neural-lineage-specific genes were augmented by loading the rSVZ-NSCExo two times with 3 days' intervals (Figure 5Bb). Unexpectedly, after loading the rSVZ-NSCExo three times with 3 days' intervals we observed a massive inhibition in neural gene expressions, possibly due to the over-saturation of cells with exosomes or exosomal contents (miRNAs and proteins) that lead trigger dysfunctional cellular behaviors[55].

3.7. Temporal and dose-dependent modulation of hMSCs by rSVZ-NSCExo: Understanding the underlying mechanism

To further corroborate the hypothesis, we obtained miRNA profiles of rSVZ-NSCExo (100 μg/mL) induced hMSCs in comparison with non-induced hMSCs. Hierarchical clustering and scattering graphs (Figure 6A,B) revealed that 54 miRNAs appeared to be significantly up/down-regulated in rSVZ-NSCExo treated hMSCs (listed in Table S3). miR-3178, miR-1469, let-7b, miR-1915, miR-762, miR-3196, miR-1908, miR-2861, miR-149, miR-4281, miR-663, miR-3195, miR-4281, miR-663, miR-3195, miR-222, miR-20a, miR-1975, miR-1228, miR-320d, miR-24, miR-424, miR-1268 were top 20 most highly up/down-regulated miRNAs. RT-qPCR analysis conducted for the two most highly up-regulated and one down-regulated miRNA (miR3178, miR1469, and miR20a) confirmed the validity of differentially expressed miRNAs identified by microarray (Figure 6C). Some of the up-regulated miRNAs (miR-3178, miR-1915, miR149, miR-663, miR-222, miR-221, and miR-181) observed in this work are also characteristic features of embryonic stem cells differentiation into neural cells[56]. In addition, four miRNAs (miR-222, miR-1268, miR-181, miR-4281) that were determined to be up-regulated in this study have been associated with neurogenic differentiation of periodontal ligament stem cells[57]. Many reports have showed that the expression of miR-181 increases with neurogenic differentiation[58-60]. Moreover, the up-regulated miR-24 in this work has been associated with neurogenic differentiation[61]. Up-regulation of these miRNAs in hMSCs after

rSVZ-NSCExo induction resembles the neural differentiation process of human adult stem cells using standard inductive factors, thus showing potential of rSVZ-NSCExo as a promising substitute for conventional exogenous inductive inductive factors.

Next, upregulated miRNAs were used to reveal the cellular pathways and processes regulated by the overexpressed miRNAs. For this, we utilized FunRich3.0 and mirPathV.3. Gene ontology analysis performed with FunRich3.0 showed that upregulated miRNAs within rSVZ-NSCExo display transcription factor activity ($p<0.001$), transcription regulator activity ($p<0.01$), and receptor binding activity ($p<0.012$) (Figure S3). Exosomal miRNAs affect the neurogenic differentiation process through regulating nucleic acid metabolism ($p<0.01$) by interacting various transcription factors including EGR1 ($p<0.001$), SP1 ($p<0.001$), SP4 ($p<0.001$), POU2F1 ($p<0.001$), SOX1 ($p<0.001$), and RREB1 ($p<0.001$) mainly in nucleus ($p<0.001$) (Figure S3). Moreover, GO analysis revealed that differentially expressed miRNAs regulate these transcriptional factors through various pathways that include TRAIL signaling pathway ($p<0.001$), IFN-g signaling pathway ($p<0.001$), ErbB receptor signaling network ($p<0.001$), Glypican-1 network ($p<0.001$), c-MET ($p<0.001$), and PDGF receptor signaling pathway ($p<0.001$) (Figure S3). In addition to FunRich3.0, we performed a GO study using mirPathV.3 to reveal KEGG pathways affected by the rSVZ-NSCExo. The results revealed that the essential target genes of the differentially expressed miRNAs were Insulin, MAPK, Wnt, Hippo, PI3K/Akt, Axon guidance, RNA degradation, and neurotrophin signaling pathways (Figure 6D). To conclude, the GO study consolidated the microarray results and supported the idea that rSVZ-NSCExo, through their miRNA content, has functions in regulating neurogenic differentiation of hMSCs.

The target biological pathways of the differentially expressed miRNAs including IFN-g signaling pathway, ErbB receptor signaling network, Glypican-1 network, c-MET, and PDGF receptor signaling pathway have previously been demonstrated to have functions in different stages of neurogenesis. IFN-g regulates the proliferation and differentiation of NSCs in SVZ[62, 63], while ErbB plays a critical role in neurogenic-specification and neuronal migration[64, 65]. In addition, Glypican-1 is expressed by NSCs[66] and controls various neurogenic processes over FGF signaling[67]. The c-MET mediates dendritic growth and synaptogenesis[68], while PDGF initiates neuronal differentiation of SVZ progenitor cells[69]. Like our GO study, others have indicated that EGR1[70], SP1[71], SP4[72], and SOX1[73] might be the underlying driver for transcript-level regulation of neural differentiation. Lastly, the use of miRPathV.3 reveals the

KEGG pathways over which rSVZ-NSCExo mediated neural-specification occurs. The Wnt[74], Hippo[75], MAPK[76], Neurotrophin[77], and PI3K/Akt[78] pathways are believed to associate with neurogenic differentiation processes.

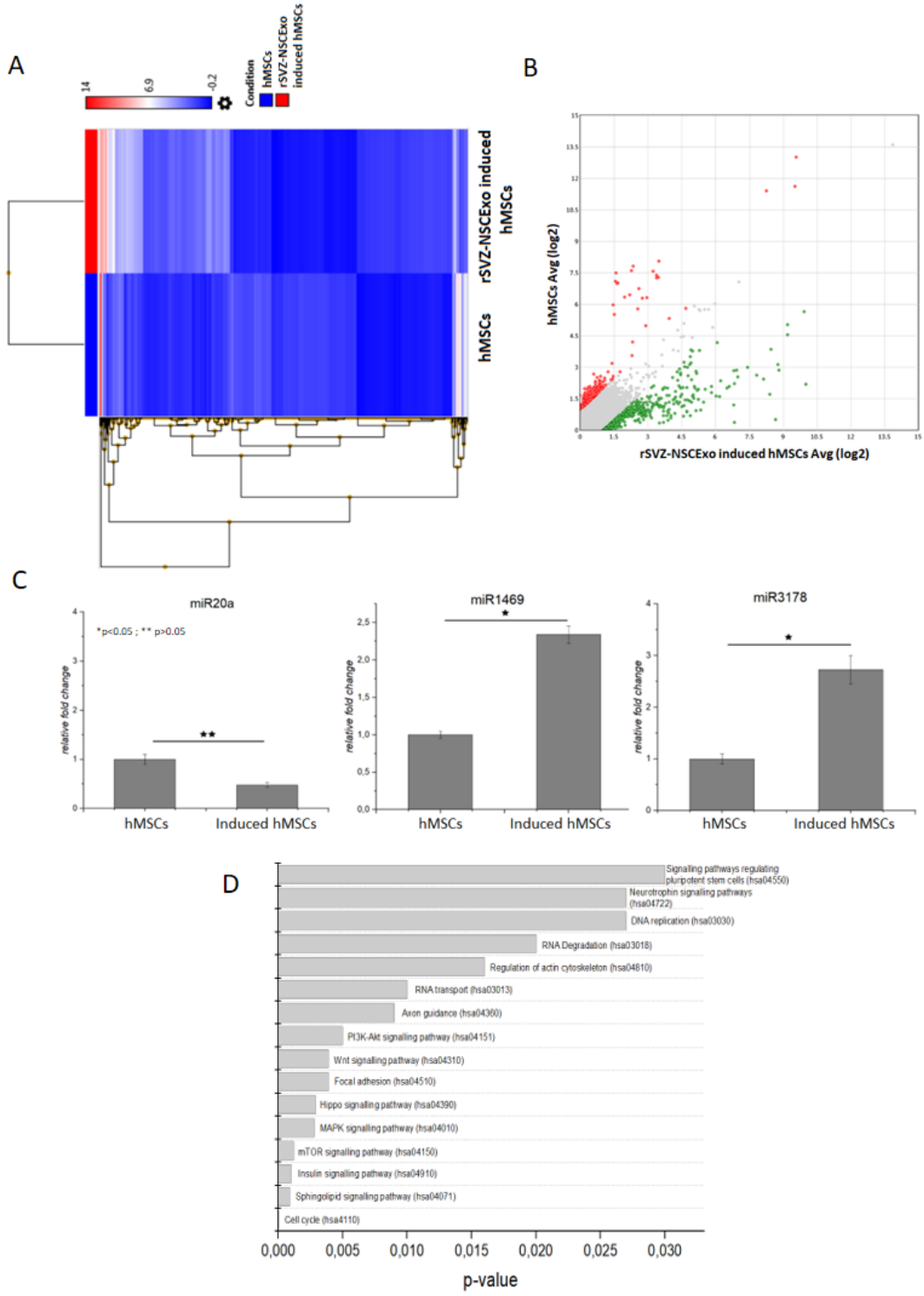

Figure 6. Assessment of the mechanism of action of rSVZ-NSCExo mediated cell reprogramming by miRNA profilling. (A) Hierachical clustering and (B) Scatter graph representing the significantly up/down regulated miRNAs in hMSCs after induction with

rSVZ-NSCExo (100 μg/mL) for 10 days (n=3).(C) Validation of two overexpressed (miR1469 and miR3178) and one down-regulated (miR20a) miRNAs by RT-qPCR. (D) KEGG pathways obtained with significantly up/down regulated miRNAs in hMSCs induced with rSVZ-NSCExo (100 μg/mL) for 10 days.

To deeply investigate the mechanism of action of rSVZ-NSCExo-mediated cell reprogramming and ultimate functions of exosomes in hMSCs, we additionally employed another high-throughput screening method namely non-targeted metabolomics. In this case, we extracted metabolites from hMSCs that were induced with 10, 50, and 100 μg/mL rSVZ-NSCExo for 10 days, and the samples were subjected to combined GC-MS and LC-MS analyses. A total of 16351 mass features were detected by LC-qTOF-MS, amongst them, 77 and 15 metabolites were identified through LC-MS and LC-MS/MS, respectively. Additionally, 424 metabolites were detected, and 62 metabolites were identified by GC-MS (data available in Excel II). The partial least squares-discriminant analysis (PLS-DA) score plot showed a remarkable discrimination between metabolic phenotypes of the three groups (Figure 7A), which was further confirmed by one-way ANOVA (Figure S4). This clear discrimination implies an altered metabolic structure in hMSCs when induced with different concentrations of rSVZ-NSCExo (10, 50, or 100 μg/mL). The most significantly altered 15 metabolites were presented in the Variable Importance in Projection (VIP) (Figure 7B). The hierarchical cluster analysis of the metabolites further depicted the changes of these metabolites between the three groups (Figure 7C). The clear pattern during the transition from 10 to 100 100 μg/mL rSVZ-NSCExo is an indication of the change in metabolome in response to rSVZ-NSCExo dose.

In addition to dose dependency, we investigated the change in metabolite profiles at different time points (1, 3, 5, and 10 days) by keeping the 100 μg/mL rSVZ-NSCExo constant (data can be found in Excel II). The production of metabolites by cells varies with time with low intragroup variation (Figure 7D), confirmed by ANOVA test (Figure S5). The most significantly altered metabolites were presented in VIP (Figure 7E), which include betaine, sorbose, myo-inositol, taurolithocholic acid, and serine, amongst others. The hierarchical clustering analysis obtained with most differentially altered metabolites demonstrated a pattern transition from day 1 to 10, asserting a temporal change in cell metabolome following the introduction of rSVZ-NSCExo (100 μg/mL). The significantly altered metabolites possibly perform their functions by affecting the pathways alanine, aspartate and glutamate metabolism, pantothenate and CoA biosynthesis, aminoacyl-tRNA biosynthesis, and citrate cycle (Figure 7G) (see Excel II) in addition to the pathways for organic cation/anion/zwitterion transport

(p=0.0026), transport of bile salts and organic acids, metal ions and amine compounds (p=0.0037), glycerophospholipid catabolism (p=0.0067), dopamine receptors (p=0.0079), inositol transporters (p=0.0032), dopamine neurotransmitter release cycle (p=0.038), and sphingolipid de novo biosynthesis (p=0.048) (obtained by Reactome.org). The interaction network of the enriched metabolites has been presented in Figure 7H. Dopamine, pyruvic acid, putrescine, taurine, and amino acids (e.g. serine, cysteine, hydroxyproline, phenyl alainine, etc.) exhibited maximum interactions with other metabolites indicating the maximum potential functional relationship with other metabolites in the network.

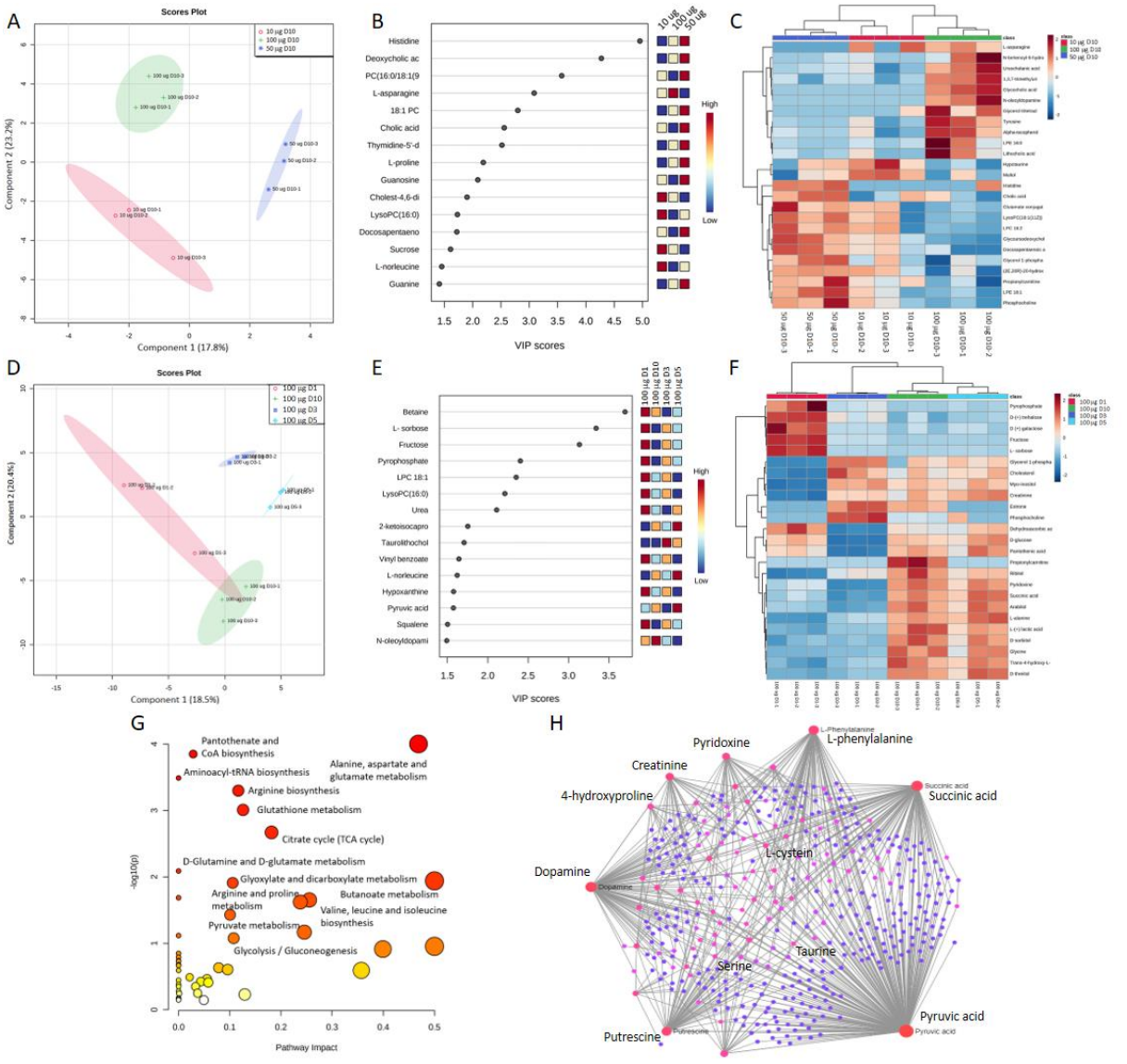

Figure 7. Untargeted metabolomics analysis for dose-dependent and temporal reprogramming of hMSCs through rSVZ-NSCExo. (A) PLS-DA diagram showing the discrimination in metabolite profile in hMSCs treated with 10, 50, and 100 100 µg/mL rSVZ-NSCExo. (B) VIP score plot and (C) Hierarchical clustering analysis obtained by altered metabolites in hMSCs that were induced with 10, 50, and 100 µg/mL rSVZ-NSCExo. (D) PLS-

DA diagram indicating the inter-group discrimination in metabolite profile in hMSCs treated with 100 μg/mL rSVZ-NSCExo for 1, 3, 5, and 10 days. (E) VIP scopre plot and (F) Hierarchical clustering heatmap graph that demonstrate the metabolite alteration patterns in hMSCs treated with 100 μg/mL rSVZ-NSCExo for 1, 3, 5, and 10 days. (G) Pathway impact graph representing the most significantly affected pathways during reprogramming process. (H) Metabolite-metabolite interaction network revealing the molecular interactions during cell reprogramming. The metabolites are represented as nodes (circles) highlighted in red in case of higher betweenness centrality followed by pink and blue in lower betweenness centrality. The size of the node indicates node degree (number of links a node has to other nodes). All analyses have been conducted by MetaboAnalyste. n=3, technical replicate=3.

To conclude, metabolomics results are consistent with the observed phenotypic change upon induction of hMSCs with various concentrations of rSVZ-NSCExo. The alteration in metabolite profile was not only dose-dependent but reconstructed by cells in time (from the initial induction time to the end of the culture duration -10 days-). This time-dependent change in metabolite profile indicates that rSVZ-NSCExo drives a temporal modulation in hMSCs to generate the new phenotype. Similar temporal alterations in metabolite profiles have previously been reported for the differentiation of MSCs into osteoblasts[79], specification of NSCs[80], reprogramming of fibroblasts into induced pluripotent stem cells (iPSCs)[81], induction of iPSCs into hepatocyte-like cells[82], and during myogenesis of skeletal muscle cells[83].

4. CONCLUSION

Mesenchymal stem cells (MSCs) have generated a great amount of enthusiasm in the past decades as a novel therapeutic paradigm for a variety of tissue regeneration due to their inherent multiple biological properties. Traditionally, MSCs are cultured on a dish or materials scaffold and induced into tissue-specific cells by supplementation with cytokines, chemokines, and growth factors. The main challenge with this induction method is whether growth-factor-induced cells resemble any stage of *in vivo* neurogenesis. Also, the reliability of the use of growth-factor-induced MSCs in regenerative medicine is questionable. To provide an alternative strategy, in this work, we examined the use of xenogenic exosomes obtained from rSVZ-derived primary NSCs in neural specification of hMSCs. The study explores the dose-dependent and temporal modulation of hMSCs by rSVZ-NSCExo and their resulting molecular change at both miRNA and metabolite levels. The ability of rSVZ-NSCExo to switch hMSCs into neuroglial cell or neural stem cell phenotype and genotype largely depends on the dose of rSVZ-NSCExo. Given the GO study obtained with miRNome data, the neural specification process is seen to proceed mainly through neural system-related pathways that include Insulin, MAPK, Wnt, Hippo, PI3K/Akt, Axon guidance, RNA degradation, and neurotrophin signaling.

In addition, a broad-range of exosomal metabolites (e.g., dopamine, betain, sphinganine, cholesterol, docosapentaenoic acid, and hypotaurine) coordinately take part in neural specification by affecting a set of pathways (e.g., organic cation/anion/zwitterion transport, transport of bile salts and organic acids, metal ions and amine compounds, glycerophospholipid catabolism, dopamine receptors, inositol transporters, dopamine neurotransmitter release cycle, and sphingolipid de novo biosynthesis). Our study shed light on the development of a novel exosome-based platform capable of reprogramming MSCs to neural-specific cells for potential application in nerve regeneration in vivo.

References

1. Kim, D. Y., Hwang, I., Muller, F. L., Paik, J. H. Functional regulation of FoxO1 in neural stem cell differentiation. *Cell Death Differ.,* **22**, 2034-2045 (2015).
2. Li, X., Zhou, W., Li, X., Gao, M., Ji, S., Tian, W., Ji, G., Du, J. And Hao, A. SOX19b regulates the premature neuronal differentiation of neural stem cells through EZH2-mediated histone methylation in neural tube development of zebrafish. *Stem Cell Research & Therapy,* **10**, 389 (2019).
3. Kaplan, D. R. and Mille, F. D. Neurotrophin signal transduction in the nervous system. *Curr.Opin.Neurobiol.,* **103**, 381-391 (2000).
4. Wang, J., Cheng, H., Li, X., Lu, W., Wang, K. and Wen, T. Regulation of neural stem cell differentiation by transcription factors HNF4-1 and MAZ-1. *Mol. Neurobiol*., **47**, 228-240 (2013).
5. Bel-Vialar, S., Medevielle, F. and Pituello, F. The on/off of Pax6 controls the tempo of neuronal differentiation in the developing spinal cord. *Dev. Biol.,* **305**, 659-673 (2007).
6. Kahn, M. A., Huang, C. J., Caruso, A., Barresi, V., Nazarian, R., Condorelli, D. F. and de Vellis, J. Ciliary neurotrophic factor activates JAK/Stat signal transduction cascade and induces transcriptional expression of glial fibrillary acidic protein in glial cells. *J. Neurochem.,* **68**, 1413-1423 (1997).
7. Zahr, S. K., Kaplan, D. R. and Miller, F. D. Translating neural stem cells to neurons in the mammalian brain. *Cell Death Differ.,* **26**, 2495-2512 (2019).
8. Baser, A., Skabkin, M., Kleber, S., Dang, Y., Gülcüler Balta, G. S., Kalamakis, G., Göpferich, M., Ibañez, D. C., Schefzik, R., Lopez, A. S., Bobadilla, E. L., Schultz, C., Fischer, B. and Martin-Villalba, A. Onset of differentiation is post-transcriptionally controlled in adult neural stem cells. *Nature,* **566**, 100-104 (2019).
9. Han, J., Kim, H. J., Schafer, S. T., Paquola, A., Clemenson, G. D., Toda, T., Oh, J., Pankonin, A. R., Lee, B. S., Johnston, S. T., Sarkar, A., Denli, A. M. and Gage, F. H. Functional Implications of miR-19 in the Migration of Newborn Neurons in the Adult Brain. *Neuron,* **91**, 79-89 (2016).
10. Szulwach, K. E., Li, X., Smrt, R. D., Li, Y., Luo, Y., Lin, L., Santistevan, N. J., Li, W., Zhao, X. and Jin, P. Cross talk between microRNA and epigenetic regulation in adult neurogenesis. *J. Cell. Biol.,* **189**, 127-141 (2010).
11. Brett, J. O., Renault, V. M., Rafalski, V. A., Webb, A. E. and Brunet, A. The microRNA cluster miR-106b~25 regulates adult neural stem/ progenitor cell proliferation and neuronal differentiation. *Aging,* **3**, 108–124 (2011).

12. de Chevigny, A., Coré, N., Follert, P., Gaudin, M., Barbry, P., Béclin, C. and Cremer, H. miR-7a regulation of Pax6 controls spatial origin of forebrain dopaminergic neurons. *Nat. Neurosci.*, **15**,1120-1126 (2012).
13. Woodbury, D., Schwarz, E. J., Prockop, D. J., Black, I. B. Adult rat and human bone marrow stromal cells differentiate into neurons. *J. Neurosci. Res.*, **61**, 364–370 (2000).
14. Hu, Y., Zhang, Y., Tian, K., Xun, C., Wang, S. and Lv, D. Effects of nerve growth factor and basic fibroblast growth factor dual gene modification on rat bone marrow mesenchymal stem cell differentiation into neuron-like cells *in vitro.* *Mol. Med. Rep.*, **13**, 49-58 (2016).
15. Sanchez-Ramos, J., Song, S., Cardozo-Pelaez, F., Hazzi, C., Stedeford, T., Willing, A., Freeman, T. B., Saporta, S., Janssen, W., Patel, N., Cooper, D. R. and Sanberg, P. R. Adult bone marrow stromal cells differentiate into neural cells in vitro. *Exp. Neurol.*, **164**, 247-56 (2000).
16. Deng, W., Obrocka, M., Fischer, I. and Prockop, D. J. Differentiation of Human Marrow Stromal Cells into Early Progenitors of Neural Cells by Conditions That Increase Intracellular Cyclic AMP. *Biochemical and Biophysical Research Communications,* **282**, 148-152 (2001).
17. Lu, Y., Yuan, X., Ou, Y., Cai, Y., Wang, S., Sun, Q. and Zhang, W. Autophagy and apoptosis during adult adiposederived stromal cells differentiation into neuron-like cells in vitro. *Neural. Regen. Res*., **7**, 1205-1212 (2012).
18. Bahls, M., Könemann, S., Markus, M. R. P., Wenzel, K., Friedrich, N., Nauck, M., Völzke, H., Steveling, A., Janowitz, D., Grabe, H. J., Felix, S. B. and Dörr, M. Brain-derived neurotrophic factor is related with adverse cardiac remodeling and high NTproBNP. *Sci. Rep*., **9**, 15421 (2019).
19. Aloe, L., Rocco, M. L., Bianchi, P. and Manni, L. Nerve growth factor: from the early discoveries to the potential clinical use. *Journal of Translational Medicine*, **10**, 1-15 (2012).
20. Jung, Y. J., Kim, H. K., Cho, Y., Choi, J. S., Woo, C. H., Lee, K. S., Sul, J. H., Lee, C. M., Han, J., Park, J. H., Jo, D. G. and Cho, Y. W. Cell reprogramming using extracellular vesicles from differentiating stem cells into white/beige adipocytes. *Sci. Adv.*, **6**, 6721 (2020).
21. Upadhya, R., Madhu, L. N., Attaluri, S., Gitaí, D. L. G., Pinson, M. R., Kodali, M., Shetty, G., Zanirati, G., Kumar, S., Shuai, B., Weintraub, S. T. and Shetty, A. K. Extracellular vesicles from human iPSC-derived neural stem cells: miRNA and protein signatures, and anti-inflammatory and neurogenic properties. *J. Extracell. Vesicles.*, **9**, 1-21 (2020).
22. Men, Y., Yelick, J., Jin, S., Tian, Y., Chiang, M. S. R., Higashimori, H., Brown, E., Jarvis, R. and Yang, Y. Exosome reporter mice reveal the involvement of exosomes in mediating neuron to astroglia communication in the CNS. *Nature Communications*, **10**, 1-18 (2019).
23. Eylem, C. C., Yilmaz, M., Derkus, B., Camci, C. B., Nemutlu, E., Yilmaz, E., Turkoglu, M. A., Aytac, B., Ozyurt, N. and Emregul, E. Untargeted Multi-Omic Analysis of Colorectal Cancer-Specific Exosomes Reveals Joint Pathways of Colorectal Cancer in both Clinical Samples and Cell Culture. *Cancer Letters*, **469**, 186-194 (2020).
24. Zhang, Z. G., Buller, B. and Chopp, M. Exosomes - beyond stem cells for restorative therapy in stroke and neurological injury. *Nature Reviews Neurology*, **15**, 193–203 (2019).
25. van Niel, G., D'Angelo, G. and Raposo, G. Shedding light on the cell biology of extracellular vesicles. *Nat. Rev. Mol. Cell. Biol*., **19**, 213-228 (2018).

26. Sharmai K. D., Schaal, D., Kore, R. A., Hamzah, R. N., Pandanaboina, S. C., Hayar, A., Griffin, R. J., Srivatsan, M., Reyna, N. S. and Xie, J. Y. Glioma-derived exosomes drive the differentiation of neural stem cells to astrocytes. *PLoS ONE,* **15**, 1-17 (2020).
27. Roballo, K. C. S., da Silveira, J. C., Bressan, F. F., de Souza, A. F., Pereira, V. M., Porras, J. E. P., Rós, F. A., Pulz, L. H., de Francisco-Strefezzil, R., dos Santos-Martins, D., Meirelles, F. V. and Ambrósio, C. E. Neurons-derived extracellular vesicles promote neural diferentiation of ADSCs: a model to prevent peripheral nerve degeneration. *Scientific Reports,* **9**, 1-11 (2019).
28. Takeda, Y. S. and Xu, Q. Neuronal Differentiation of Human Mesenchymal Stem Cells Using Exosomes Derived from Differentiating Neuronal Cells. *PLoS One,* **10**, 1-15 (2015).
29. Narayanan, K., Kumar, S., Padmanabhan, P., Gulyas, B., Wan, A. C. A. and Rajendran, V. M. Lineage-specific exosomes could override extracellular matrix mediated human mesenchymal stem cell differentiation. *Biomaterials*, **182**, 312-322 (2018).
30. Lan, W. R., Pan, S., Li, H. Y., Sun, C., Chang, X., Lu, K., Jiang, C. Q., Zuo, R., Zhou, Y. and Li, C.Q. Inhibition of the Notch1 Pathway Promotes the Effects of Nucleus Pulposus Cell-Derived Exosomes on the Differentiation of Mesenchymal Stem Cells into Nucleus Pulposus-Like Cells in Rats. *Stem Cells Int.*, **2019**, 1-12 (2019).
31. Huang, C. C., Narayanan, R., Alapati, S. and Ravindran, S. Exosomes as biomimetic tools for stem cell differentiation: Applications in dental pulp tissue regeneration. *Biomaterials*, **111**, 103-115 (2016).
32. Ma, Y., Li, C., Huang, Y., Wang, Y., Xia, X. and Zheng, J. C. Exosomes released from neural progenitor cells and induced neural progenitor cells regulate neurogenesis through miR-21a. *Cell Communication and Signaling*, **17**, 1-10 (2019).
33. Rong, Y., Liu, W., Wang, J., Fan, J., Luo, Y., Li, L., Kong, F., Chen, J., Tang, P. and Cai, W. Neural stem cell-derived small extracellular vesicles attenuate apoptosis and neuroinflammation after traumatic spinal cord injury by activating autophagy. *Cell Death and Disease*, **10**, 1-18 (2019).
34. Morton, M. C., Neckles, V. N., Seluzicki, C. M., Holmberg, J. C. and Feliciano, D. M. Neonatal Subventricular Zone Neural Stem Cells Release Extracellular Vesicles that Act as a Microglial Morphogen. *Cell Reports*, **23**, 78–89 (2018).
35. Morton, M. C., Neckles, V. N. and Feliciano, D. M. Isolation of Extracellular Vesicles from Subventricular Zone Neural Stem Cells. In: Turksen K. (eds) Stem Cell Niche. *Methods in Molecular Biology*, **2002,** 75-85 (2018).
36. Guo, W., Patzlaff, N. E., Jobe, E. M. and Zhao, X. Isolation of multipotent neural stem or progenitor cells from both the dentate gyrus and subventricular zone of a single adult mouse. *Nature Protocols*, **7**, 2005-2012 (2012).
37. Lee, A., Kessler, J. D., Read, T. A., Kaiser, C., Corbeil, D., Huttner, W. B., Johnson, J. E. and Wechsler-Reya R. J. Isolation of neural stem cells from the postnatal cerebellum. *Nature Neuroscience*, **8**, 723– 729 (2005).
38. Jmorrison, S., White, P. M., Zock, C. and Anderson, D. J. Prospective Identification, Isolation by Flow Cytometry, and In Vivo Self-Renewal of Multipotent Mammalian Neural Crest Stem Cells. *Cell*, **96**, 737-749 (1999).
39. Liu, A., Chen, X., Bao, L., Liu, T., Yuan, P., Yang, X., Qui, X., Gooding, J. J., Bai, Y., Xiao, J., Pu, F. and Jin, Y. Treatment of infarcted heart tissue via the capture and local delivery of circulating exosomes through antibody-conjugated magnetic nanoparticles. *Nature Biomedical Engineering*, **4**, 1063–1075 (2020).
40. Du, W., Zhang, K., Zhang, S., Wang, R., Nie, Y., Tao, H., Han, Z., Liang, L., Wang, D., Liu, J., Liu, N., Han, Z., Kong, D., Zhao, Q. and Li, Z. Enhanced proangiogenic

potential of mesenchymal stem cell-derived exosomes stimulated by a nitric oxide releasing polymer. *Biomaterials*, **133**, 70-81 (2017).
41. Kim, H., Kang, J. Y., Mun, D., Yun, N. and Joung, B. Calcium chloride enhances the delivery of exosomes. *PLoS ONE*, **14**, (2017).
42. Zhang, G., Zhu, Z., Wang, H., Yu, Y., Chen, W., Waqas, A., Wang, Y. and Chen, L. Exosomes derived from human neural stem cells stimulated by interferon gamma improve therapeutic ability in ischemic stroke model. *J. Adv. Res.*, **24**, 435-445 (2020).
43. Yang, S., Guo, S., Tong, S. and Sun, X. Promoting Osteogenic Differentiation of Human Adipose-Derived Stem Cells by Altering the Expression of Exosomal miRNA. *Stem Cells International*, **2019**, 1-15 (2019).
44. Höglinger, G. U., Rizk, P., Muriel, M. P., Duyckaerts, C., Oertel, W. H., Caille, I. and Hirsch, E. C. Dopamine depletion impairs precursor cell proliferation in Parkinson disease. *Nat. Neurosci.*, **7**, 726-35 (2004).
45. Peden, A. S., Mac, P., Fei, Y. J., Castro, C., Jiang, G., Murfitt, K. J., Miska, E. A., Griffin, J. L., Ganapathy, V. and Jorgensen, E. M. Betaine acts on a ligand-gated ion channel in the nervous system of the nematode C. elegans. *Nat. Neurosci.*, 16, 1794-801 (2013).
46. Ko, M., Zou, K., Minagawa, H., Yu, W., Gong, J. S., Yanagisawa, K. and Michikawa, M. Cholesterol-mediated Neurite Outgrowth Is Differently Regulated between Cortical and Hippocampal Neurons. *Journal of Biological Chemistry*, **280**, 42759-42765 (2005).
47. Mauch, D. H., Nägler, K., Schumacher, S., Göritz, C., Müller, E. C., Otto, A. and Pfrieger, F. W. CNS synaptogenesis promoted by glia-derived cholesterol. *Science*, **294**, 1354-7135 (2001).
48. Lee, C. W., Lee, T. V., Chen, V. C., Bui, S. and Riechman, S. Dietary Cholesterol Affects Skeletal Muscle Protein Synthesis Following Acute Resistance Exercise. *The Faseb Journal*, **25**, 563-563 (2011).
49. Kilb, W. and Fukuda, A. Taurine as an Essential Neuromodulator during Perinatal Cortical Development. *Front. Cell Neurosci*.,**11**, 1-13 (2017).
50. Jun, Y. J., Kim, H. K., Cho, Y., Choi, J. S., Woo, C. H., Lee, D. S., Sul, J. H., Lee, C. M., Han, J., Park, J. H., Jo, D. G. and Cho, Y. W. Cell reprogramming using extracellular vesicles from differentiating stem cells into white/beige adipocytes. *Science Advances*, **6**, 1-13 (2020).
51. Ma, Y., Li, C., Huang, Y., Wang, Y., Xia, X. and Zheng, J. C. Exosomes released from neural progenitor cells and induced neural progenitor cells regulate neurogenesis through miR-21a. *Cell Communication and Signaling*, **17**, 1-10 (2019).
52. Stronati, E., Conti, R., Cacci, E., Cardarelli, S., Biagioni, S. and Poiana, G. Extracellular Vesicle-Induced Differentiation of Neural Stem Progenitor Cells. *Int. J. Mol. Sci.*, **20**, 1-10 (2019).
53. Mao, Q., Nguyen, P. D., Shanti, R. M., Shi, S., Shakoori, P., Zhang, Q. and Le, A. D. Gingiva-Derived Mesenchymal Stem Cell-Extracellular Vesicles Activate Schwann Cell Repair Phenotype and Promote Nerve Regeneration. *Tissue. Eng. Part A*, **25**, 887-900 (2019).
54. Wilson, H. K., Canfield, S. G., Hjortness, M. K., Palecek, S. P. and Shusta, E. V. Exploring the effects of cell seeding density on the differentiation of human pluripotent stem cells to brain microvascular endothelial cells. *Fluids Barriers CNS*, **12**, 1-12 (2015).
55. Grimm, D., Streetz, K. L., Jopling, C. L., Storm, T. A., Pandey, K., Davis, C. R., Marion, P., Salazar, F. and Kay, M. A. Fatality in mice due to oversaturation of cellular microRNA/short hairpin RNA pathways. *Nature*, **441**, 537-541 (2006).

56. Liu, J., Githinji, J., Mclaughlin, B., Wilczek, K. and Nolta, J. Role of miRNAs in neuronal differentiation from human embryonic stem cell-derived neural stem cells. *Stem Cell Rev. Rep*., **8**, 1129-1137 (2012).
57. Ng, T. K., Yang, Q., Fortino, V. R., Lai, N. Y., Carballosa, C. M., Greenberg, J. M., Choy, K. W., Pelaez, D., Pang, C. P. and Cheung, H. S. MicroRNA-132 directs human periodontal ligament-derived neural crest stem cell neural differentiation. *J. Tissue Eng. Regen. Med*., **13**, 12-24 (2019).
58. Stappert, L., Borghese, L., Roese-Koerner, B., Weinhold, Philipp Koch, S., Terstegge, Markus Uhrberg S., Wernet, P. and Brüstle, O. MicroRNA-Based Promotion of Human Neuronal Differentiation and Subtype Specification. *PLOS ONE*, **8**, 1-12 (2013).
59. Parsons, X. H., Parsons, J. F. and Moore, D. A. Genome-Scale Mapping of MicroRNA Signatures in Human Embryonic Stem Cell Neurogenesis. *Mol. Med. Ther.*, **10** (2012).
60. Wei, Z. J., Fan, B. O., Liu, Y., Ding, H., Tang, H. S., Pan, D. Y., Shi J., Zheng, P., Shi, H., Wu, H., Li, A. and Feng, S. MicroRNA changes of bone marrow-derived mesenchymal stem cells differentiated into neuronallike cells by Schwann cell-conditioned medium. *Neural. Regen. Res*., **14**, 1462-1469 (2019).
61. Kang M., Park, S. and Han, J. MicroRNA-24-3p regulates neuronal differentiation by controlling hippocalcin expression. *Cellular and Molecular Life Sciences*, **76**, 4569–4580 (2019).
62. Pereira, L., Medina, R., Baena, M., Planas. A. M. and Pozas, E. IFN gamma regulates proliferation and neuronal differentiation by STAT1 in adult SVZ niche. *Front. Cell. Neurosci.,* **9** (2015).
63. Warre-Cornish, K., Perfect, L., Nagy, R., Duarte, R. R. R., Reid, M. J., Raval, P., Mueller, A., Evans, A. L., Couch, A., Ghevaert, C., McAlonan, G., Loth, E., Murphy, D., Powell, T. R., Vernon, A. C., Srivastava, D. P. and Price, J. Interferon-γ signaling in human iPSC-derived neurons recapitulates neurodevelopmental disorder phenotypes. *Sci. Adv.,* **6** (2020).
64. Galvez-Contreras, A. Y., Quiñones-Hinojosa, A. and Gonzalez-Perez, O. The role of EGFR and ErbB family related proteins in the oligodendrocyte specification in germinal niches of the adult mammalian brain. *Front. Cell. Neurosci.,* **7** (2013).
65. Rio, C., Rieff, H. I., Qi, P., Khurana, T. S. and Corfas, G. Neuregulin and erbB receptors play a critical role in neuronal migration. *Neuron.*, **19**, 39-50 (1997).
66. Abaskharoun, M., Bellemare, M., Lau, E. and Margolis, R. U. Glypican-1, phosphacan/receptor protein-tyrosine phosphatase-ζ/β and its ligand, tenascin-C, are expressed by neural stem cells and neural cells derived from embryonic stem cells. *ASN Neuro.*, **2** (2010).
67. Jen, Y. H., Musacchio, M. and Lander, A. D. Glypican-1 controls brain size through regulation of fibroblast growth factor signaling in early neurogenesis. *Neural Dev*., **4** (2019).
68. Eagleson, K. L., Lane, C. J., McFadyen-Ketchum, L., Solak, S., Wu, H. H. and Levitt, P. Distinct intracellular signaling mediates C-MET regulation of dendritic growth and synaptogenesis. *Dev. Neurobiol.*, **76**, 1160-1181 (2016).
69. Williams, B. P., Park, J. K., Alberta, J. A., Muhlebach, S. G., Hwang, G. Y., Roberts, T. M. and Stiles, C. D. A PDGF-regulated immediate early gene response initiates neuronal differentiation in ventricular zone progenitor cells. *Neuron.*, **18**, 553-562 (1997).
70. Adams, K. W., Kletsov, S., Lamm, R. J., Elman, J. S., Mullenbrock, S. and Cooper, G. M. Role for Egr1 in the Transcriptional Program Associated with Neuronal Differentiation of PC12 Cells. *PLoS One*, **12** (2017).

71. Mondanizadeh, M., Arefian, E., Mosayebi, G., Saidijam, M., Khansarinejad, B. and Hashemi, S. M. MicroRNA-124 regulates neuronal differentiation of mesenchymal stem cells by targeting Sp1 mRNA. *J. Cell. Biochem.*, **116**, 943-953 (2015).
72. Santos, M. C., Tegge, A. N., Correa, B. R., Mahesula, S., Kohnke, L. Q., Qiao, M., Ferreira, M. A., Kokovay, E. and Penalva, L. O. miR-124, -128, and -137 Orchestrate Neural Differentiation by Acting on Overlapping Gene Sets Containing a Highly Connected Transcription Factor Network. *Stem Cells*, **34**, 220-232 (2016).
73. Ahmad, A., Strohbuecker, S., Tufarelli, C. and Sottilev, V. Expression of a SOX1 overlapping transcript in neural differentiation and cancer models. *Cell Mol. Life Sci.*, **74**, 4245–4258 (2017).
74. Kondo, T., Matsuoka, A. J., Shimomura, A., Koehler, K. R., Chan, R. J., Miller, J. M., Srour, E. F. and Hashino, E. Wnt signaling promotes neuronal differentiation from mesenchymal stem cells through activation of Tlx3. *Stem Cells*, **29**, 836-846 (2011).
75. Tzeng, H. H., Hsu, C. H., Chung, T. H., Lee, W. C., Lin, C. H., Wang, W. C., Hsiao, C. Y., Leu, Y. W. and Wang, T. H. Cell Signaling and Differential Protein Expression in Neuronal Differentiation of Bone Marrow Mesenchymal Stem Cells with Hypermethylated Salvador/Warts/Hippo (SWH) Pathway Genes. *PLoS One*, **10** (2015).
76. Zheng, B., Wang, C., He, L., Xu, X., Qu, J., Hu, J. and Zhang, H. Neural differentiation of mesenchymal stem cells influences chemotactic responses to HGF. *J. Cell Physiol.*, **228**, 149-162 (2013).
77. Brick, R. M., Sun, A. X. and Tuan, R. S. Neurotrophically Induced Mesenchymal Progenitor Cells Derived from Induced Pluripotent Stem Cells Enhance Neuritogenesis via Neurotrophin and Cytokine Production. *Stem Cells Transl. Med.*, **7**, 45-58 (2018).
78. Peng, L., Shu, X., Lang, C. and Yu, X. Cardiotrophin-1 stimulates the neural differentiation of human umbilical cord blood-derived mesenchymal stem cells and survival of differentiated cells through PI3K/Akt-dependent signaling pathways. *Cytotechnology*, **69**, 933-941 (2017).
79. Klontzas, M. E., Vernardis, S. I., Heliotis, M., Tsiridis, E. and Mantalaris, A. Metabolomics Analysis of the Osteogenic Differentiation of Umbilical Cord Blood Mesenchymal Stem Cells Reveals Differential Sensitivity to Osteogenic Agents. *Stem Cells Dev.*, **26**, 723-733 (2017).
80. Marin-Navarro, A., Pronk, R. J., van der Geest, A. T., Oliynyk, G., Nordgren, A., Arsenian-Henriksson, M., Falk, A. and Wilhelm, M. p53 controls genomic stability and temporal differentiation of human neural stem cells and affects neural organization in human brain organoids. *Cell Death Dis.*, **11** (2020).
81. Park, S. J., Lee, S. A., Prasain, N., Bae, D., Kang, H., Ha, T., Kim, J. S., Hong, K. S., Mantel, C., Moon, S. H., Broxmeyer, H. E. and Lee, M. R. Metabolome Profiling of Partial and Fully Reprogrammed Induced Pluripotent Stem Cells. *Stem Cells Dev.*, **26**, 734-742 (2017).
82. Jellali, R., Bernier, M. L., Tauran, Y., Gilard, F., Danov, M., Kido, T., Miyajima, A., Sakai, Y. and Leclerc, E. Metabolomic profiling during the differentiation of human induced pluripotent stem cells into hepatocyte-like cells. Differentiation, **112**, 17-26 (2020).
83. Kumar, A., Kumar, Y., Sevak, J. K., Kumar, S., Kumar, N. and Gopinath, S. D. Metabolomic analysis of primary human skeletal muscle cells during myogenic progression. *Sci. Rep.*, **10** (2020).

Acknowledgements

This work was financially supported by the Scientific and Technological Research Council of Turkey (TUBITAK) with the grant number 116S476.

Author contributions

B.D. and E.E. conceived and designed the study. B.D. and I.E. dissected SVZ tissues from rats. B.D. and Y.E.A. isolated and characterized NSCs. B.D. and M.I. performed in vitro cell culture experiments. C.C., S.B., and M.A. performed exosome isolation and characterization. F.K. supervised gene expression study. C.C.C. and E.N. performed metabolomics and bioinformatics studies. O.A. and Ç.E. supervised exosome isolation and characterization. B.O.O. made data curing, reviewed-revised the manuscript.

Competing interests

The authors declare no competing interest.